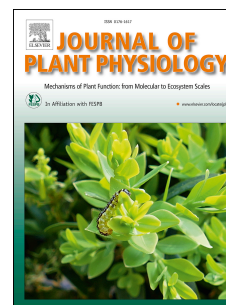# Journal Pre-proof

Suppression of metabolite shuttles for export of chloroplast and mitochondrial ATP and NADPH increases the cytosolic NADH: NAD+ ratio in tobacco leaves in the dark

Beatriz Moreno-García, Patricia E. López-Calcagno, Christine A. Raines, Lee J. Sweetlove

Please cite this article as: Moreno-García, B., López-Calcagno, P.E., Raines, C.A., Sweetlove, L.J., Suppression of metabolite shuttles for export of chloroplast and mitochondrial ATP and NADPH increases the cytosolic NADH: NAD+ ratio in tobacco leaves in the dark, *Journal of Plant Physiology* (2021), doi: https://doi.org/10.1016/j.jplph.2021.153578.

This is a PDF file of an article that has undergone enhancements after acceptance, such as the addition of a cover page and metadata, and formatting for readability, but it is not yet the definitive version of record. This version will undergo additional copyediting, typesetting and review before it is published in its final form, but we are providing this version to give early visibility of the article. Please note that, during the production process, errors may be discovered which could affect the content, and all legal disclaimers that apply to the journal pertain.

Beatriz Moreno-García: Conceptualization, Methodology, Experiments, Formal Analysis, Writing – Original Draft, Writing – Review and Editing
Patricia E. López-Calcagno: Experiments, Writing – Review and Editing
Christine A. Raines: Resources, Writing – Review and Editing, Supervision
Lee J. Sweetlove: Conceptualization, Methodology, Writing – Original Draft, Writing – Review and Editing, Supervision

Title: Suppression of metabolite shuttles for export of chloroplast and mitochondrial ATP and NADPH increases the cytosolic NADH: NAD$^+$ ratio in tobacco leaves in the dark

Authors: Beatriz Moreno-García[1,3]*, Patricia E. López-Calcagno[2], Christine A. Raines[2], Lee J. Sweetlove[1]

Addresses:
[1]Department of Plant Sciences, University of Oxford, South Parks Road, Oxford, OX1 3RB, UK
[2]School of Life Sciences, University of Essex, Wivenhoe Park, Colchester, CO4 3SQ, UK
[3]Current address: School of Life Sciences, University of Essex, Wivenhoe Park, Colchester, CO4 3SQ, UK
*Corresponding author: beatriz.morenogarcia@essex.ac.uk, +44 (0) 7719293431

Abstract
The communication between chloroplasts and mitochondria, which depends on the inter-organellar exchange of carbon skeletons, energy, and reducing equivalents, is essential for maintaining efficient respiratory metabolism and photosynthesis. We devised a multi-transgene approach to manipulate the leaf energy and redox balance in tobacco (*Nicotiana tabacum*) while monitoring the *in vivo* cytosolic redox status of NAD(H) using the biosensor c-Peredox-mCherry. Our strategy involved altering the shuttling capacity of the chloroplast by (1) increasing the chloroplast malate valve capacity by overexpression of the chloroplast malate valve transporter pOMT from Arabidopsis (*AtpOMT1)* while (2) reducing the activity of the chloroplast triose-phosphate/3-phosphoglycerate shuttle by knocking down the cytosolic NAD-dependent glyceraldehyde 3-phosphate dehydrogenase (*NtGAPC*). This was accompanied by (3) alterations to the export of reducing equivalents in the mitochondria by knocking down the mitochondrial malate dehydrogenase (*NtmMDH)* and (4) an increased expression of the mitochondrial fission regulator FIS1A from Arabidopsis (*AtFIS1A).* The multi-transgene tobacco plants were analysed in glasshouse conditions and showed significant increases in the cytosolic NADH:NAD$^+$ in the dark when transcript levels for *NtGAPC* or *NtmMDH* were knocked down. In addition, principal component analysis and Spearman correlation analyses showed negative correlations between average transcript levels for the gene targets and parameters related to chlorophyll fluorescence and plant growth. Our results highlight the importance of the shuttling of energy and reducing equivalents from chloroplasts and mitochondria to support photosynthesis and growth and suggest an important role for the dual 2-oxoglutarate/malate and oxaloacetate/malate transporter (pOMT).

Keywords:
organelle communication, energy balance, redox metabolism, plant metabolic engineering, multi-transgene transformation, *Nicotiana tabacum*

Abbreviations
- 3-PGA: 3-phosphoglycerate
- AOX: alternative oxidase
- CBB: Calvin-Benson-Bassham
- FIS1A: fission regulator FISSION1A
- GAPC: phosphorylating NAD-dependent glyceraldehyde 3-phosphate dehydrogenase
- gFW: grams of fresh weight
- mC: mCherry
- mETC: mitochondrial electron transport chain
- mMDH: mitochondrial malate dehydrogenase
- OAA: oxaloacetate
- OCR: oxygen consumption rate

- PC: principal component
- PCA: principal component analysis
- pOMT: plastidic, dual 2-oxoglutarate/malate and oxaloacetate/malate transporter
- TCA: tricarboxylic acid
- TPT: triose-phosphate/phosphate translocator
- Ts: T-Sapphire

Acknowledgements

Suppression of metabolite shuttles for export of chloroplast and mitochondrial ATP and NADPH increases the cytosolic NADH: NAD⁺ ratio in tobacco leaves in the dark

Introduction

Photosynthesis is considered the most important process in the biogeosphere in terms of carbon flux (Beer *et al.*, 2010), converting inorganic CO_2 into triose phosphates in chloroplasts, ultimately used as carbon skeletons for plant growth. However, 30-40% of assimilated carbon is subsequently lost as CO_2, principally due to respiration, but also other metabolic decarboxylations (Amthor, 2010; Sweetlove *et al.*, 2013; Xu *et al.*, 2021). Respiration entails flux through glycolysis, the oxidative pentose phosphate pathway, the tricarboxylic acid (TCA) cycle and the mitochondrial electron transport chain (mETC) (McDonald and Vanlerberghe, 2007). Re-oxidation of photoassimilates to CO_2 by respiration occurs mainly in the dark and provides energy (ATP), reducing power (NAD(P)H) and carbon skeletons for metabolism and transport processes underpinning growth and maintenance. Mitochondria also have important functions that contribute to the maintenance of photosynthetic rates in the light, mainly dissipation of excess reducing equivalents generated by the photochemical reactions, which are oxidised by the mETC (Padmasree, Padmavathi and Raghavendra, 2002; Noctor, De Paepe and Foyer, 2007; Dahal *et al.*, 2017; Alber and Vanlerberghe, 2019).

Photosynthetic and respiratory metabolism are highly intertwined, which implies a high degree of inter-organellar cross-talk. This communication depends on the exchange of energy, reducing equivalents, and carbon skeletons across organelle membranes via specific translocators or metabolite shuttles (Kromer, 1995). While there are specific mitochondrial and chloroplast ATP-ADP translocators, metabolite shuttles such as the chloroplast and mitochondrial malate valves, which transfer reducing equivalents, are thought to be of particular importance for redox homeostasis during photosynthesis (Selinski and Scheibe, 2019). Additionally, the chloroplast triose-phosphate/3-phosphoglycerate (3-PGA) shuttle can contribute to the export of ATP and NADH to the cytosol via the triose-phosphate/phosphate translocator (TPT) (Häusler *et al.*, 2000; Schneider *et al.*, 2002; Gardeström and Igamberdiev, 2016).

Experimental investigations over the last decades suggest organelle communication between chloroplasts and mitochondria is essential for maintaining the redox and energy balance in plant cells. These investigations have used both pharmacological and genetic approaches. For example, chemical inhibitors of respiration have been used to determine the degree of respiratory activity during photosynthesis. Application of oligomycin, an inhibitor of mitochondrial ATP synthase, and rotenone, an inhibitor of mitochondrial complex I, both delayed photosynthetic induction in barley (*Hordeum vulgare*) protoplasts (Igamberdiev *et al.*, 1998). Similarly, application of the alternative oxidase (AOX) inhibitor salicylhydroxamic acid in pea (*Pisum sativum*) decreased the light activation of Calvin-Benson-Bassham (CBB) cycle enzymes the chloroplast NADP malate dehydrogenase (Padmasree and Raghavendra, 2001). Genetic perturbation showed impairment of complex I of the mETC in *Nicotiana sylvestris* was associated with slower photosynthetic induction (Dutilleul *et al.*, 2003).

The use of genetic approaches highlighted the interdependence between chloroplast and mitochondrial metabolism. The barley *albolstrians* mutant, deficient in plastid ribosomes, shows increased mitochondrial gene copies and transcript levels (Hedtke *et al.*, 1999), suggesting an enhanced mitochondrial activity in response to chloroplast defects. Transgenics and mutants in TCA cycle genes have different effects on photosynthesis (Nunes-Nesi, Sweetlove and Fernie, 2007). Reductions in the activity of aconitase in tomato (*Solanum lycopersicum*) and succinate dehydrogenase in tomato and Arabidopsis (*Arabidopsis thaliana*) increased photosynthesis (Carrari

et al., 2003; Araújo *et al.*, 2011; Fuentes *et al.*, 2011), while the antisense targeting of fumarase reduced photosynthesis and biomass due to reduced stomatal conductance in tomato (Nunes-Nesi *et al.*, 2007). Tomato mutants in mitochondrial malate dehydrogenase (mMDH) showed improvements in photosynthesis and growth under long-day regime (Nunes-Nesi *et al.*, 2005) but dwarfism under short-day conditions (Nunes-Nesi *et al.*, 2008). Arabidopsis double knockout mutants in mMDH showed photorespiratory alterations, with reductions in net CO_2 assimilation and growth rates caused by a redox imbalance in the shuttling of NADH between mitochondria and peroxisomes (Tomaz *et al.*, 2010; Lindén *et al.*, 2016).

The effect of the alterations of mitochondrial respiratory proteins on photosynthesis is not limited to the TCA cycle but includes proteins that are not dependent on adenylate control. For example, overexpression of AOX had a photoprotective effect under drought conditions in wheat (*Triticum aestivum*) (Bartoli *et al.*, 2005) and tobacco (*Nicotiana tabacum*) (Dahal and Vanlerberghe, 2018). An Arabidopsis T-DNA insertional mutant in *AtUCP1* encoding mitochondrial uncoupling protein revealed a photosynthetic phenotype due to a reduced oxidation of photorespiratory glycine in mitochondria (Sweetlove *et al.*, 2006), while overexpression of *AtUCP1* in tobacco led to the up-regulation of genes from photosynthetic electron transport, including photosystem II assembly and transport through photosystem I (Laitz *et al.*, 2015), and seed yield increases mediated by increases in respiration and photosynthesis (Barreto *et al.*, 2017).

While it is clear that communication between chloroplasts and mitochondria is essential for photosynthetic activity, the mechanisms coordinating this interaction have not been fully elucidated. A number of genetically-encoded fluorescence sensors have arisen that improve our ability to monitor *in vivo* inter-organellar metabolite exchange in plants (Schwarzländer *et al.*, 2016; Smith *et al.*, 2021). Biosensors have been developed to monitor the redox status of thioredoxin, NAD(H), NADP(H), glutathione and oxygen peroxide (Müller-Schüssele, Schwarzländer and Meyer, 2021), as well as MgATP^{2-}(De Col *et al.*, 2017), with a recent system developed for the simultaneous monitoring of the cytosolic redox dynamics of ATP, calcium, pH, and the NAD and glutathione redox status in plants (Wagner *et al.*, 2019). The ratiometric sensor c-Peredox-mCherry, which reports the cytosolic status of the redox couple NADH/NAD$^+$ (Hung et al., 2011), has been used to determine dynamic changes in NADH/NAD$^+$ in different cells and tissues in Arabidopsis in response to light, inhibitors of mitochondrial respiration, sugar supply, and elicitors (Steinbeck *et al.*, 2020). The combination of the fluorescent protein sensors iNAP and SoNar to monitor changes in NADPH and the NADH/NAD$^+$ ratio between compartments in Arabidopsis led to the finding that the mETC is unable to dissipate the excess photorespiratory NADH, emphasising the role of the mitochondrial malate-oxaloacetate (OAA) shuttle in exporting excess reducing equivalents (Lim *et al.*, 2020). The *in vivo* dynamics of ATP in chloroplasts and the cytosol have been investigated using a MgATP^{2-} Förster resonance energy transfer (FRET) sensor in Arabidopsis, suggesting chloroplasts import little cytosolic ATP to support the CBB cycle and rather balance the NADPH/ATP ratios by exporting reducing equivalents (Voon *et al.*, 2018).

In addition, computational models have emerged as a valuable tool that captures the complexity of the metabolic network, allowing a systems-level perspective (Baghalian, Hajirezaei and Schreiber, 2014). Recently, a computational model of leaf primary metabolism in Arabidopsis explored the contributions of chloroplasts and mitochondria to the leaf energetic balance. A diel flux balance analysis, accounting for dark and night conditions, under different scenarios of light conditions and energy utilisation suggested a major role for photorespiratory glycine in providing NADPH for mitochondrial ATP production and for the malate valve and other shuttles in supplying cytosolic reactions with reducing equivalents to achieve a balanced energy status (Shameer, Ratcliffe and Sweetlove, 2019).

A tight energetic coupling between chloroplasts and mitochondria has been described in diatoms (Bailleul *et al.*, 2015), where the exchange of ATP and reducing equivalents between chloroplasts and mitochondria were found to be crucial to ensure the fuelling of carbon assimilation. Recently, a

combined transgenic and chemical inhibitor approach was performed to explore if this organelle energy coupling occurs in angiosperms (Alber and Vanlerberghe, 2021). Using tobacco AOX knockdown and overexpressing lines, the authors showed a high degree of interactions between chloroplasts and mitochondria upon application of photosynthetic or respiratory inhibitors, highlighting the role for mitochondrial metabolism as a sink for excess reductant generated during photosynthesis.

We conceived a metabolic engineering strategy to further investigate inter-organellar energy and redox coupling by simultaneously targeting multiple connection points between chloroplast-cytosol and cytosol-mitochondria energy and reducing equivalent shuttles in tobacco (Figure 1). We hypothesised that an increased capacity of the chloroplast malate valve that shuttles reducing equivalents from the chloroplast (Hatch *et al.*, 1984; Sweetlove *et al.*, 2007; Gardeström and Igamberdiev, 2016; Shameer, Ratcliffe and Sweetlove, 2019), while at the same time reducing the capacity of the triose-phosphate/3-PGA shuttle by supressing cytosolic NAD-dependent glyceraldehyde 3-phosphate dehydrogenase (GAPC), would perturb the energy and redox balance of the system. This is because the latter shuttle exports both reducing equivalents and ATP from the chloroplast, while the malate valve only exports reducing equivalents. In principle, the flexibility and robustness of the energy coupling mechanisms in the leaf (Alber and Vanlerberghe, 2021) should be able to adjust for any potential ATP shortfall in the cytosol as a result of these changes. The main expected mechanism would be for the mitochondrion to supply additional ATP by oxidation of photorespiratory NADH. However, it is generally thought that the amount of NADH generated within the mitochondrion during photorespiration exceeds the capacity of the cytochrome respiratory chain, hence the requirement for alternative and uncoupling electron transport pathways in the mitochondrion (Gardeström and Igamberdiev, 2016; Lim *et al.*, 2020; Vanlerberghe *et al.*, 2020). Nevertheless, stoichiometric modelling suggests that more complete utilisation of this NADH resource for oxidative phosphorylation would be more efficient (Shameer, Ratcliffe and Sweetlove, 2019). To address this, one of our gene targets was the overexpression of the *FISSION1A* gene that controls mitochondrial division and is known to increase total number of mitochondria in Arabidopsis leaves (Zhang and Hu, 2008). Alongside this, we elected to supress the expression of *mMDH* to reduce mitochondrial NAD-malate dehydrogenase activity and thereby reduce the transfer of reducing equivalents from mitochondrion to cytosol (and vice versa) via malate-OAA shuttling (the mitochondrial equivalent of the chloroplast malate valve). In order to monitor the effect of these changes on the redox balance within the cell, we included the genetically encoded fluorescent redox biosensor c-Peredox-mCherry (Hung *et al.*, 2011) in our multigene construct. c-Peredox-mCherry localises to the cytosol and is based on a circularly permuted fluorescent protein, the blue-green fluorescent protein T-Sapphire (Ts), and a bacterial NADH and NAD^+-binding protein, T-Rex. When the biosensor interacts with NADH, conformational coupling between fluorescence and binding takes place, with an increase in the fluorescence of Ts, while binding of NAD^+ has no impact on fluorescence emission intensity. The sensor includes an additional fluorescent protein, mCherry (mC), which allows for internal fluorescence normalisation. Therefore, the ratio of fluorescence emission of Ts over mC provides a relative, ratiometric measurement of the concentration of NADH to NAD^+ in the cytosol. As it has previously been shown that perturbations to both mitochondrial and chloroplast bioenergetics are transmitted to the redox state of the cytosolic $NADH/NAD^+$ couple, and that these perturbations can be detected by c-Peredox-mCherry (Steinbeck *et al.*, 2020), this represents a facile way to get monitor the extent of energy and redox balance perturbation our transgenes caused.
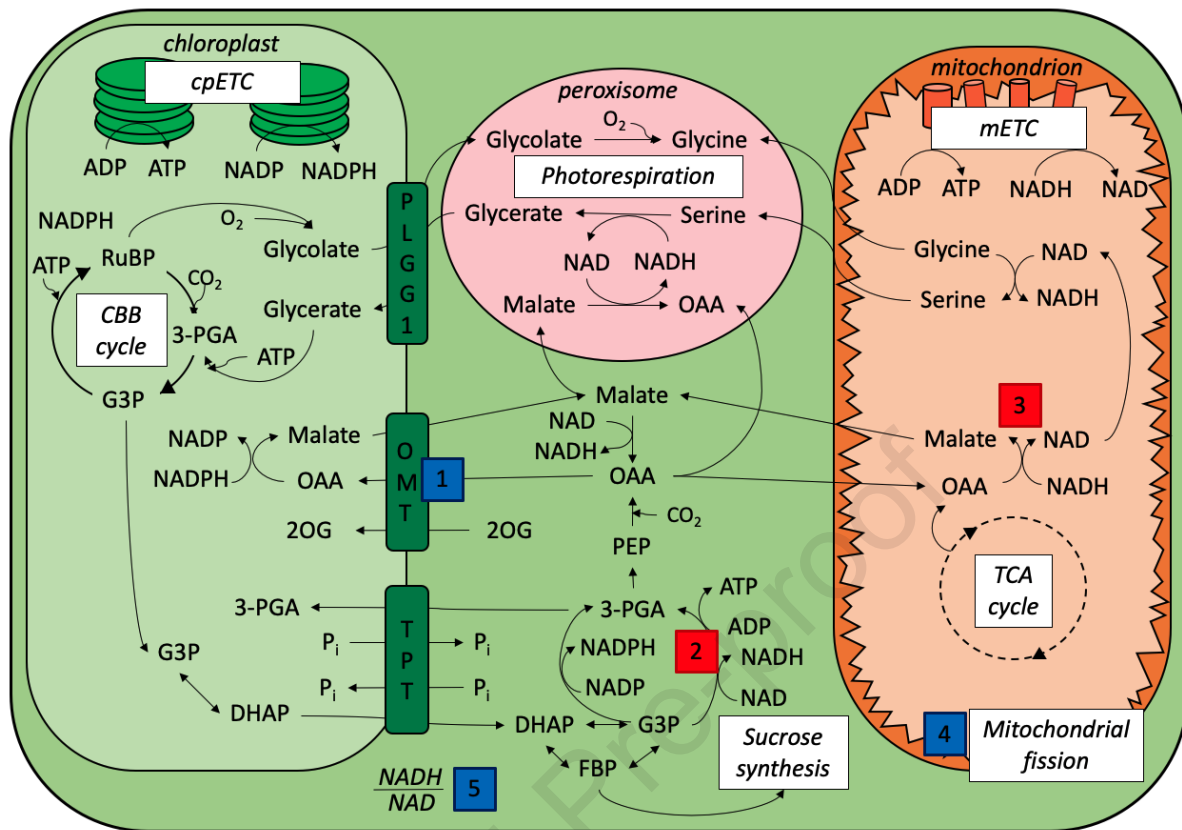
[COLOUR: PRINT AND ONLINE] **Figure 1: Schematic representation of the cross-talk between organelles in a mesophyll cell and the genes targeted by a multi-transgene approach in tobacco**. Genes targeted in this work are labelled with a box, coloured in blue (overexpression) and red (antisense repression). **1**: *AtpOMT1*, Arabidopsis plastidic 2-oxoglutarate/malate transporter. **2**: *NtGAPC*, tobacco cytosolic glyceraldehyde 3-phosphate dehydrogenase. **3**: *NtmMDH*, tobacco mitochondrial malate dehydrogenase. **4**: *AtFIS1A*, Arabidopsis mitochondrial fission regulator. **5**: *c-Peredox-mCherry*: genetically encoded fluorescent biosensor reporting cytosolic NADH/NAD$^+$ ratios. Abbreviations: 2OG: 2-oxoglutarate; 3-PGA: 3-phosphoglycerate; ADP: adenosine diphosphate; ATP: adenosine 5'-triphosphate; CBB: Calvin-Benson-Bassham; CO_2: carbon dioxide; cpETC: chloroplast electron transport chain; DHAP: dihydroxyacetone phosphate; FBP: fructose 1,6-bisphosphate; G3P: glyceraldehyde 3-phosphate; mETC: mitochondrial electron transport chain; NAD(H): nicotinamide adenine dinucleotide; NADP(H): Nicotinamide adenine dinucleotide phosphate; O_2: oxygen; OAA: oxaloacetate; OMT: dual 2-oxoglutarate/malate and oxaloacetate/malate transporter; PEP: phosphoenolpyruvate; P_i: inorganic phosphate; PLGG1: plastidic glycolate glycerate transporter; RuBP: ribulose 1,5-bisphosphate; TCA: tricarboxylic acid; TPT: triose-phosphate/phosphate translocator.

Materials and methods

Sequence retrieval of target genes

Arabidopsis contains two genes encoding GAPC (*GAPC1*, AT3G04120 and *GAPC2*, AT1G13440) and two genes encoding mMDH (*mMDH1*, AT1G53240 and *mMDH2*, AT3G15020). The protein sequences encoded by these genes in Arabidopsis were retrieved from The Arabidopsis Information Resource (*https://www.arabidopsis.org*) and used to identify the corresponding tobacco orthologues using the BLAST tool against the tobacco genome at the Sol Genomics Network database (Fernandez-Pozo *et al.*, 2015). For mMDH, four DNA sequences were found with a percentage identity of over 80%, regardless of which Arabidopsis gene was used for the search. Eleven hits with percentage identities of over 80% were found in the case of the GAPC sequences, when using either *AtGAPC1* or *AtGAPC2*. It was thus not possible to distinguish between orthologues and the tobacco sequences with highest similarity to the Arabidopsis sequences were retrieved: mRNA_105100 (gene_62994, 1026 bp) for *NtmMDH* and mRNA_81739 (gene_48071, 984 bp) for *NtGAPC*.

Vector construction

Constructs were generated using Golden Gate cloning (Engler, Kandzia and Marillonnet, 2008; Engler *et al.*, 2009; Weber *et al.*, 2011) and the Plant Modular Cloning toolbox (Engler *et al.*, 2014). Reverse complement DNA sequences were used to design antisense constructs for *NtmMDH* and *NtGAPC*. DNA fragments for *NtmMDH* (639 bp) and *NtGAPC* (487 bp) were amplified from tobacco cDNA using primers NtmMDHf (5'- CACTCTGTGGTCTCAAATGTGTCACAGTTGACTGCACGAATGAACACTC-3'), NtmMDHr (5'- CACTTCGTGGTCTCAAAGCACACCAGATCTCAGGTTTCTGGGTTTGC -3'), NtGAPCf (5'- CACTCTGTGGTCTCAAATGCCCTCCACAATTCCAAACCT-3') and NtGAPCr (5'- CACTTCGTGGTCTCAAAGCGGATTGGTCGTTTGGTGGCAAGAGTT-3') and purified to generate the antisense constructs driven by leaf-specific *SlRbcS2* and *StLS1* promoters, respectively. DNA corresponding to *AtpOMT1* (AT5G12860), *AtFIS1A* (AT3G57090), and *c-Peredox-mCherry* (Hung *et al.*, 2011; Steinbeck *et al.*, 2020) genes, flanked by Golden Gate adapter sites, was artificially synthesised by Bio Basic (Ontario, Canada) and placed under the control of leaf specific promoters *AtRbcS2B* and *AtLHB1B1*, and the constitutive *2xCaMV35S* promoter, respectively. These transcriptional units were used to build a multi-transgene construct, LS0201, in a plant binary vector pAGM4723. An additional construct, LS0207, was built using the *c-Peredox-mCherry* transcriptional unit. Both constructs included a hygromycin phosphotransferase gene as selection marker.

Plant transformation and growth

The recombinant plasmids LS0201 and LS0207 were introduced into six-week-old tobacco (*Nicotiana tabacum* cv. Petit Havana SR1) plants using *Agrobacterium tumefaciens* strain LBA4404 via leaf-disc transformation (Horsch *et al.*, 1985). Shoots were regenerated on MS medium containing hygromycin (20 mg L^{-1}), and cefotaxime (400 mg L^{-1}). Hygromycin-resistant primary transformants (T$_0$ generation) with established root systems were transferred to soil and allowed to self-fertilize. Forty-seven lines were generated carrying the multi-transgene construct LS0201 and 53 carrying LS0207.

The T$_1$ seeds were germinated on antibiotic-containing media for two weeks to select for transgenic plants (hetero- and homozygous) before transfer to soil. Growth chamber conditions (Sanyo mlR-350H, Sanyo, Osaka, Japan) consisted of a long day photoperiod of 16 h of light and 8 h of dark and a day/night temperature cycle of 22 °C/14 °C. Transgenic plants were grown in containment glasshouses at the Department of Plant Sciences, University of Oxford, Oxford (UK), with long-day photoperiod conditions (natural light supplemented to give an irradiance of up to 200 μmol (photons) m^{-2} s^{-1}) and a day/night temperature cycle of 22 °C/18 °C. Soil composition consisted of a mixture of Levington M2 compost and vermiculite (3:1), along with 0.4 g L^{-1} of the insecticide Exemptor (ICL, Ipswich, UK). Square (9 cm each side), black, plastic pots were used. Soil was kept

moistened with regular watering. Water was supplemented weekly with a standard fertiliser, Miracle Gro (Scotts Miracle-Gro Company, OH, USA), for development of primary tobacco transformants (T$_0$).

Total RNA extraction and cDNA synthesis

For total RNA extraction, 300-400 mg samples of frozen powdered plant material were prepared with the TRIzol reagent (Thermo Fisher Scientific, MA, USA), following the manufacturer's instructions. The extracted RNA pellet was treated with DNase I (TURBO DNA-Free Kit, Ambion, Thermo Fisher Scientific, MA, USA). After spectrophotometric quantification, 0.5 µg of RNA was used for cDNA synthesis using the SuperScript IV Reverse Transcriptase (Thermo Fisher Scientific, MA, USA).

Quantitative real-time PCR analyses

Quantitative real-time PCR (qRT-PCR) was performed in a StepOnePlus system (Thermo Fisher Scientific, MA, USA) using 1 µL of cDNA as template in 20 µL reactions containing 10 µL of the 2X qPCRBIO SyGreen Mix HI-ROX (PCR Biosystems, London, UK), corresponding primers (Supplementary Table 1), and ddH$_2$O. Two or three technical replicates were analysed per plant. Results were normalised to the average of the mRNA levels of the housekeeping genes *L25 ribosomal protein* (*L25*) and *Elongation Factor-1α* (*EF-1α*) (Schmidt and Delaney, 2010). Relative transcript levels were determined as $2^{-\Delta\Delta Ct}$ as per Pfaffl (Pfaffl, 2001).

Plant growth measurements

Plant growth was evaluated by measuring plant height, leaf number, and fresh biomass. Plant height was determined from the base to the top of the shoot. Determination of fresh weight aboveground biomass involved all aerial tissues, including leaves, the main and lateral shoots, flowers, and flower buds. Stem biomass included inflorescences, where present.

OJIP fluorescence transient

Chlorophyll *a* fluorescence- based analysis was performed using a PAR-FluorPen FP 110 (Photon Systems Instruments, Drasov, Czech Republic) pulsed amplitude modulation fluorometer. The youngest fully expanded leaf of each plant was dark-adapted for 20 min with a detachable leaf clip. Surfaces of dark-adapted leaves were exposed to a super pulse of blue light (455 nm) for 1 s to induce an OJIP transient fluorescence rise, with an intensity of ~ 900 µmol (photons) m^{-2} s^{-1}. The OJIP protocol included the following measured parameters: F$_0$, fluorescence intensity at 50 µs; F$_j$, fluorescence intensity at J-step (2 ms); F$_i$ fluorescence intensity at I-step (30 ms); and F$_m$, maximum fluorescence intensity. From these, a number of estimated parameters were calculated as per Strasser, Srivastava and Tsimilli-Michael (Strasser, Srivastava and Tsimilli-Michael, 2000).

Analyses of dark respiration

An oxygen consumption assay was developed for tobacco leaf discs following (Sew, Harvey Millar and Stroeher, 2015; O'Leary *et al.*, 2017), with modifications. The Seahorse Bioscience XFe24 Extracellular Flux Analyser (Seahorse Bioscience, MA, USA) was used to determine real-time fluorimetric detection of oxygen levels in a microtiter plate, measured as oxygen consumption rates (OCR). Leaf discs (5 mm-diameter) were excised from the youngest fully expanded leaf. Cyanoacrylate super glue (Gorilla Super Glue Gel, Gorilla Glue Europe, Chorley, UK) was used to attach the leaf discs (abaxial side up) to the bottom of the wells. One mL of respiration buffer (50 mM hydroxyethyl piperazineethanesulfonic acid, 10 mM 2-(N-morpholino)ethanesulfonic acid, and 2 mM CaCl$_2$ (pH 6.6, adjusted with NaOH)) was added to each well (Sew *et al.*, 2013; O'Leary *et al.*, 2017). Plates were kept in the dark for 1 h. Sensor cartridge calibration was done following the manufacturer's instructions. A 30 min wait step was included between the calibration and measurement steps to ensure stabilisation of OCR. The protocol consisted of three steps: mix (3

min), wait (2 min), measure (3 min). The OCR of single leaf discs was recorded by the Wave software version 2.6.0.31 (Agilent Technologies, CA, USA) and fresh weight was used to calculate normalised OCR values. Each 24-well plate contained four discs per line, coming from the youngest fully expanded leaf of an independent plant. Four wells were used as blanks to determine the background levels of OCR, containing glue and 1 mL of respiration buffer. Single-gene transgenic plants overexpressing the c-Peredox-mCherry biosensor and WT plants were used as control lines.

Quantitation of the cytosolic NADH/NAD$^+$ redox poise using the cPeredox-mCherry sensor protein

The fluorescence emission spectra of the ratiometric c-Peredox-mCherry sensor was used to determine the *in vivo* status of the redox couple NADH/NAD$^+$ using a plate reader fluorimetry assay, based on Steinbeck *et al.* (Steinbeck *et al.*, 2020), with modifications. Three-week-old transgenic plants carrying the c-Peredox-mCherry sensor and WT control plants were used. Leaf discs (6-mm diameter), each corresponding to a different plant, were laid at the bottom of each well (abaxial face up) in Nunclon 96-well, flat-bottom, transparent microplates (Thermo Fisher Scientific, MA, USA). A total volume of 200 µL assay medium (10 mM 2-(N-morpholino)ethanesulfonic acid, 5 mM KCl, 10 mM MgCl$_2$, 10 mM CaCl$_2$, pH 5.8 adjusted with KOH) was added to each well. Plates were kept in the dark for 2 h before recording fluorescence to minimise potential effects of active photosynthesis. The fluorophores Ts and mC were excited at 400 ± 9 nm and 570 ± 9 nm, respectively, and emission collected at 520 ± 20 nm and 610 ± 20 nm in a Tecan Infinite 200 (Tecan, Zurich, Switzerland) using top optics, well-multichromatic monitoring, 25 flashes per well, and measuring cycle with orbital averaging. The gain was manually set as 162 for Ts and 188 for mC to allow data to be compared between different experiments. Each experiment was independently repeated twice, and the results of both experiments were averaged.

Data analysis

Statistical analyses were performed using R (R Development Core Team, 2013) in RStudio version 1.2.5033 (RStudio Team, 2020). Statistical differences between groups were determined using one-way analysis of variance (ANOVA; *res.aov* function) followed by post hoc Tukey test (*TukeyHSD* function). The R packages *FactoMineR* (for data analysis) and *factoextra* (for data visualisation) were used to perform principal component analysis (PCA). For the PCA, data were scaled and missing values were imputed using the *missMDA* package. Spearman correlation tests were done using the *ggscatter* function from the *ggpubr* package. Figure preparation was done using the R packages *ggplot2* and *ggpubr*.

Results

Selection of gene targets and generation of multi-transgene tobacco plants

To realise an inter-organellar energy and redox balance perturbation (Figure 1), we designed and assembled a multi-transgene construct, LS0201, using Golden Gate technology (Engler, Kandzia and Marillonnet, 2008; Engler *et al.*, 2009, 2014; Weber *et al.*, 2011). LS0201 carried overexpression cassettes for the Arabidopsis *AtFIS1A and AtpOMT* genes and the redox biosensor c-Peredox-mCherry (Hung *et al.*, 2011) and antisense, silencing cassettes for the tobacco genes *NtmMDH* and *NtGAPC*. *AtFIS1A* (AT3G57090) encodes the outer mitochondrial membrane protein FISSION1A and its overexpression was shown to lead to increases in mitochondrial number (Zhang and Hu, 2008, 2009). *AtpOMT1* (AT5G12860) encodes the chloroplast dual 2-oxoglutarate/malate and oxaloacetate/malate transporter (Taniguchi *et al.*, 2002; Kinoshita *et al.*, 2011) and is a key component of the chloroplast malate valve (Taniguchi and Miyake, 2012). *NtmMDH* encodes the mitochondrial malate dehydrogenase (Tomaz *et al.*, 2010; Lindén *et al.*, 2016). *NtGAPC* is considered a key chloroplast source of ATP in the cytosol (Rius *et al.*, 2008; Gardeström and Igamberdiev, 2016). In addition, the multi-transgene construct included the sequence coding for the c-Peredox-mCherry biosensor, which allowed for integration of the metabolic redox dynamics and visualisation of NAD coupling between cell compartments (Hung *et al.*, 2011). *NtmMDH*, *NtGAPC*, *AtFIS1A*, *AtpOMT1* were placed under the control of light-responsive promoters from the MoClo Plant Parts Kit (Engler *et al.*, 2014): *pSlRbcS2*, *pStLS1*, *pAtRbcS2B*, and *pAtLHB1B1*, respectively. Promoters were chosen based on their strength in previously published *Agrobacterium*-mediated transfection experiments (Engler *et al.*, 2014). The use of a diversity of promoters has been reported to reduce the risk of transcriptional gene silencing resulting from sequence homology (Peremarti *et al*. 2010). c-Peredox-mCherry was placed under the control of the constitutive promoter *p2xCaMV35S.*

An additional construct was generated, LS0207, carrying an overexpression cassette for c-Peredox-mCherry only that served as a control to monitor the NADH:NAD$^+$ ratio in otherwise WT plants. The recombinant plasmids LS0201 and LS0207 (Figure 2) were introduced into tobacco. Forty-seven lines were generated carrying the multi-transgene construct LS0201 and 53 carrying LS0207, containing the biosensor only. The T$_1$ progeny of the primary transformants, a mix of homo- and heterozygous plants, were used to examine the effects of the multi-transgene approach in tobacco. The 47 lines carrying the multi-transgene construct LS0201 were analysed in three subsequent batches, each including 15-16 lines. Another four lines, carrying the construct LS0207, containing the redox biosensor c-Peredox-mCherry only, were grown alongside the multi-transgene lines and used as transformed controls. These lines were selected based on strong fluorescence from the expressed biosensor. Plants were germinated on hygromycin-selection plates and antibiotic-resistant seedlings were grown in controlled glasshouse conditions.

[COLOUR: PRINT AND ONLINE] **Figure 2. Schematic representation of the T-DNA part of the transgene constructs LS0201 and LS0207 introduced in tobacco via *Agrobacterium* transformation.** LS0201, a multi-transgene constrict, was used to induce a shift in inter-organellar energy and redox balance. LS0207, a construct containing the redox sensor c-Peredox-mCherry, was used to generate control plants with basal sensor fluorescence. **Promoters**: *pAtLHB1B1*, Arabidopsis light-harvesting chlorophyll-protein complex II subunit B1 promoter; *pAtRbcS2B*, Arabidopsis RuBisCO small subunit (*RbcS*) promoter 2B; *pCaMV35S*, CaMV 35S promoter; *p2xCaMV35S*, double-enhancer CaMV 35S promoter; *pSlRbcS2*, *S. lycopersicum* (tomato) RbcS2 promoter; *pStLS1*, *S. tuberosum* (potato) leaf and stem-specific promoter. Yellow colouring indicates constitutive promoters, green indicates photosynthetic-specific promoters. **Genes/fragments**: Arabidopsis fission regulator 1A (*AtFIS1A*); Arabidopsis plastidic 2-oxoglutarate/malate transporter (*AtpOMT1*); antisense fragment for the tobacco cytosolic NAD-dependent glyceraldehyde 3-phosphate dehydrogenase (*NtGAPC*); antisense fragment for the tobacco mitochondrial malate dehydrogenase (*NtmMDH*); hygromycin phosphotransferase (*Hygromycin-B*). Blue colouring indicates sense orientation, red indicates antisense orientation. **Terminators**, grey colouring: Arabidopsis heat shock protein 18.2 terminator (*hsp18.2-T*); nopaline synthase terminator (*NosT*). **Other features**: the left (LB) and right (RB) borders for *Agrobacterium*-mediated T-DNA transfer are indicated in light blue colouring. **Backbone**: Golden Gate level 2 terminal acceptor, plant binary vector *pAGM4723*.
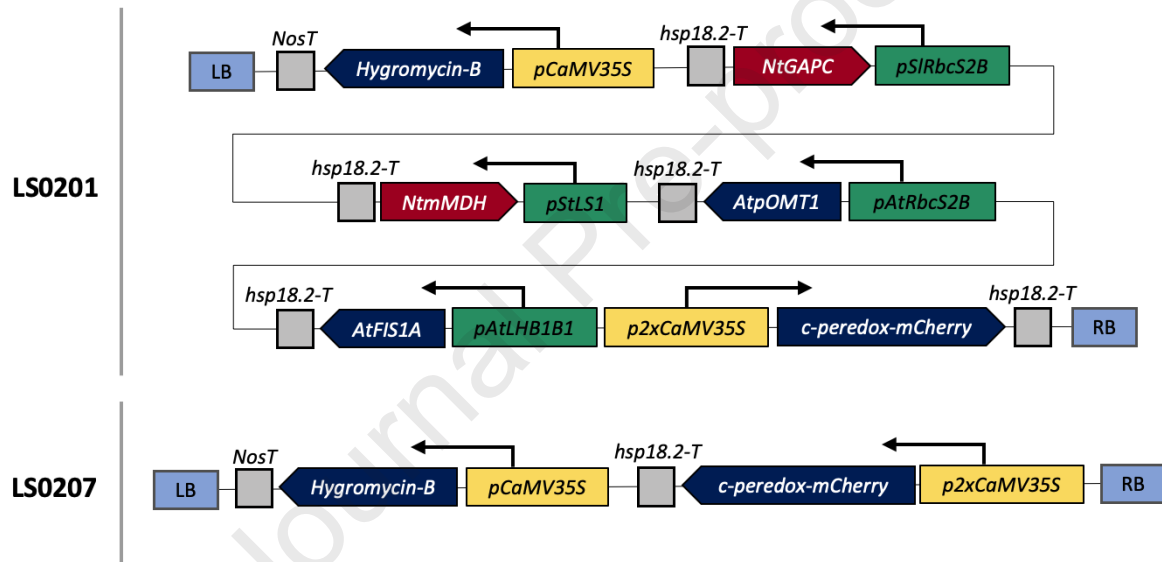
Gene expression analysis reveals variability among transgenic lines transformed with the multi-transgene construct LS0201

The multi-transgene tobacco plants were analysed for gene expression, respiratory and photosynthetic capacity, plant growth, and the NAD(H) redox status. Relative transcript levels were determined for the endogenous genes *NtGAPC* and *NtmMDH* and the transgenes *AtFIS1A* and *AtpOMT1* using qRT-PCR in multi-transgene plants of the T_1 generation. Despite all transgenic lines carrying the same construct, LS0201, transcript levels of individual gene targets varied considerably between lines and within plants of the same line due to the segregation the T_1 tobacco progeny (Supplementary Table 2). Therefore, we decided to classify plants into expression groups based on transcript levels of the different transgenes, regardless of the line to which they belonged (Figure 3). Plants with mRNA levels at least 25% lower than the WT ($2^{-\Delta\Delta Ct}$ < 0.75) for *NtGAPC* or *NtmMDH* were considered knock-down mutants and plants where mRNA levels ($2^{-\Delta\Delta Ct}$ > 4) for *AtFIS1A* and *AtpOMT1* were detected were considered overexpressors (e.g. plants labelled as 'GMFO' showed silencing of *NtGAPC* (G) and *NtmMDH* (M) and overexpression of *AtFIS1A* (F) and *AtpOMT1* (O), while lines in the 'MFO' group showed silencing of *NtmMDH* only and overexpression of *AtFIS1A* and *AtpOMT1*). The WT controls used in the three experimental batches were compared and no differences were found between them, so all the WT plants were combined into a single control group (Supplementary Table 3). The classification into expression groups based on transcript levels for the target genes was used for the rest of analyses.

[COLOUR: PRINT AND ONLINE] Figure 3. Relative transcript levels of target genes in expression groups of LS0201 tobacco multi-transgenic tobacco plants. A. Relative transcript levels, represented as mRNA levels, $(2^{-\Delta\Delta Ct})$ were determined by quantitative real-time PCR (qRT-PCR) in leaves, relative to the transcript levels of the housekeeping genes *L25* (L25 ribosomal protein) and *EF-1α* (elongation factor 1-α). Average transcript levels and standard error are given for each expression group. **B.** Expression groups consisted of: plants with reduced transcript levels (knock-down) of *NtGAPC* (labelled as G), *NtmMDH* (M), or both (GM); plants with increased transcript levels (overexpression) of *AtFIS1A* (F) or *AtFIS1A* and *AtpOMT* (Flow_Olow, Flow_Ohigh, Fhigh_Olow, Fhigh_Ohigh); and plants with a combination of reduced transcripts for *NtGAPC* and/or *NtmMDH* and overexpression of *AtFIS1A* and *AtpOMT* (GFO, MFO, GMFO). The number of plants (N) in each expression group is indicated. Abbreviations: *AtFIS1A*, mitochondrial fission regulator; *AtpOMT1*, plastidic 2-oxoglutarate/malate transporter; *c-Peredox-mCherry*: cytosolic fluorescent sensor of NADH/NAD+ ratio; *NtGAPC*, cytosolic glyceraldehyde 3-phosphate dehydrogenase; *NtmMDH*, mitochondrial malate dehydrogenase.
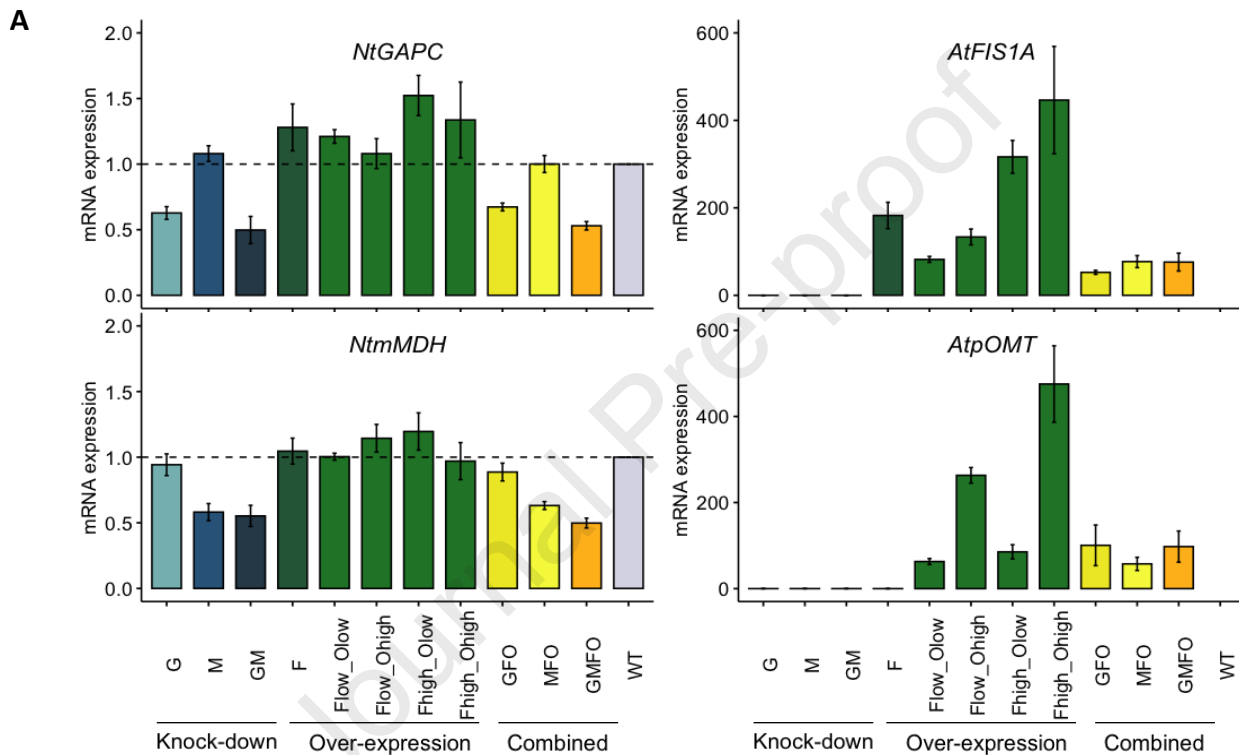

Expression group			Transcript levels			
Colour	Name	N	*NtGAPC*	*NtmMDH*	*AtFIS1A*	*AtpOMT*
	G	4	Reduced	Unchanged	Absent	Absent
	M	6	Unchanged	Reduced	Absent	Absent
	GM	4	Reduced	Reduced	Absent	Absent
	F	5	Unchanged	Unchanged	Increased	Absent
	Flow_Olow	46	Unchanged	Unchanged	Increased, low	Increased, low
	Flow_Ohigh	5	Unchanged	Unchanged	Increased, low	Increased, high
	Fhigh_Olow	7	Unchanged	Unchanged	Increased, high	Increased, low
	Fhigh_Ohigh	3	Unchanged	Unchanged	Increased, high	Increased, high
	GFO	3	Reduced	Unchanged	Increased	Increased
	MFO	14	Unchanged	Reduced	Increased	Increased
	GMFO	19	Reduced	Reduced	Increased	Increased
	WT	20	Unchanged	Unchanged	Absent	Absent

The multi-transgene tobacco lines did not show significant changes in chlorophyll fluorescence, dark respiration and growth

Photosynthetic capacity was evaluated using an OJIP chlorophyll fluorescence transient in the youngest fully expanded leaf, five weeks after transfer to soil, using a PAR-FluorPen FP 110. Maximum quantum efficiency of PS II photochemistry (F_v/F_m, Figure 4.A) and other OJIP-derived chlorophyll fluorescence parameters (not shown) did not differ between expression groups and the 'Peredox' and WT controls. Mitochondrial respiration was evaluated by measuring leaf disc oxygen consumption rates (OCR) in a multi-well microplate using a Seahorse XFe24 Extracellular Flux Analyser. No changes were observed between expression groups when measuring leaf disc respiration (Figure 4.B). Expression groups did not show significant differences in terms of total aerial biomass with respect to the controls (Figure 4.C).

[COLOUR: PRINT AND ONLINE] Figure 4. Analyses of chlorophyll fluorescence, plant growth, and dark respiratory capacity in the multi-transgene tobacco plants. Photosynthetic quantum yield (F_v/F_m, **A**) was determined with a PAR-FluorPen FP 110 (Photon Systems Instruments, Drasov, Czech Republic) on five-week-old plants. Respiratory capacity (**B**) was determined as leaf disc oxygen consumption rates (OCR) using a Seahorse XFe24 Extracellular Flux Analyser (Seahorse Bioscience, MA, USA) on four- week-old plants. Total, fresh-weight aerial biomass (**C**) was measured on six-week-old plants. Plants carrying the LS0207 construct, labelled as 'Peredox', along with WT plants, were included as controls. Data represent the mean of the expression group ± standard error. Colouring represents groups based on transcript levels, as per Figure 3. Significant changes between groups were identified by one-way ANOVA, followed by post hoc Tukey multiple pairwise comparisons test. P-values are as follows: F_v/F_m, 0.006; biomass, 0.249; OCR, 0.074.
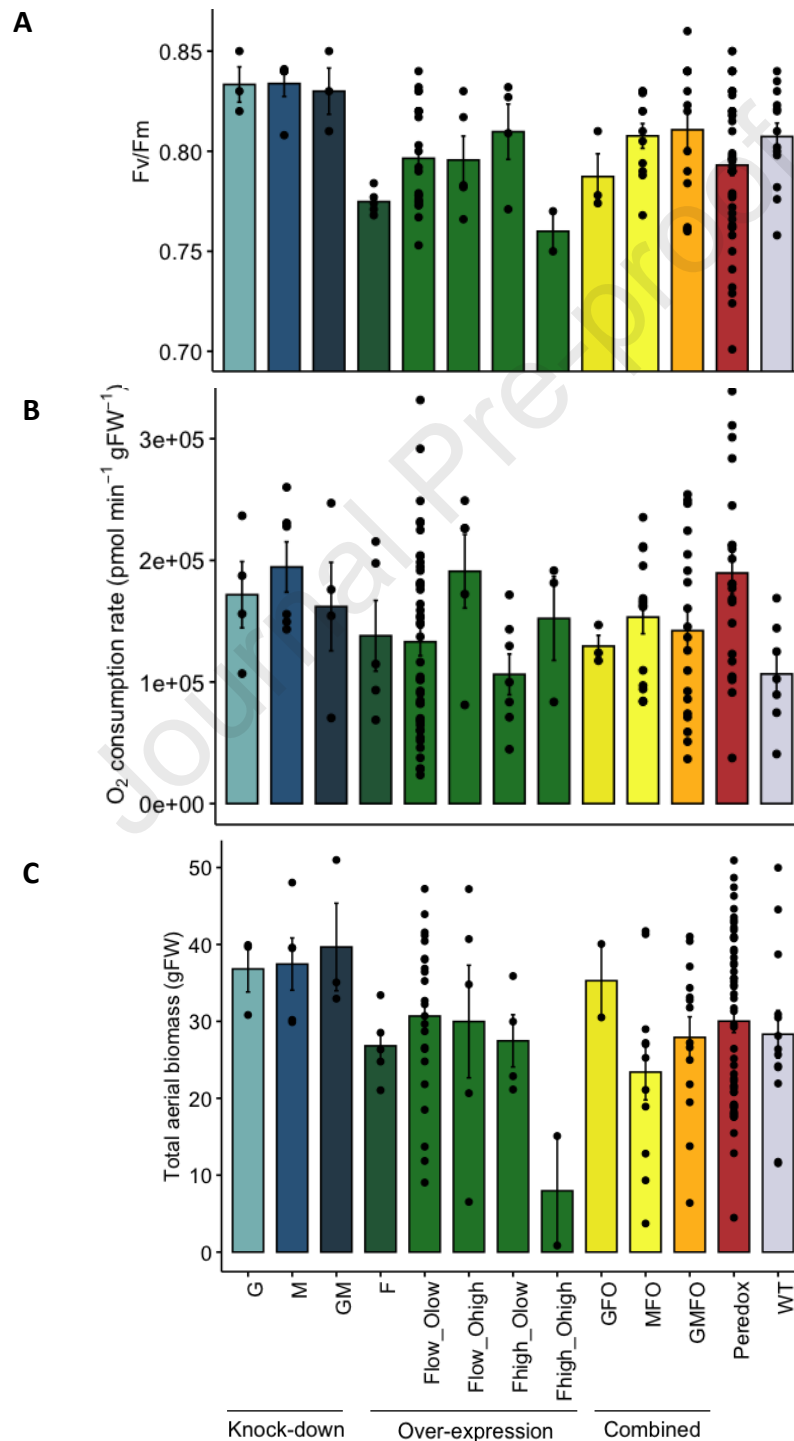
Transgenic lines where *NtGAPC* or *NtmMDH* were suppressed showed significant changes in their cytosolic NAD(H) redox status

The dark *in vivo* redox status of NADH/NAD$^+$ was evaluated in leaf discs using a plate reader fluorimetry assay (Wagner *et al.*, 2019; Steinbeck *et al.*, 2020). Fluorescence emission was collected from Ts and mC and used as a proxy for the cytosolic NADH to NAD$^+$ ratio. The ratio values of Ts/mC were log$_{10}$ transformed to accurately represent the ratio variance and to restore the symmetry of ratio data. The 'Peredox' control plants showed low NADH/NAD$^+$ ratios (-0.18 on average), in line with previous analyses of the *in vivo* redox status of c-Peredox-mCherry in Arabidopsis leaves (Steinbeck *et al.*, 2020). The redox status showed variability between expression groups and within plants of the same group (Figure 5). While most plants had NADH/NAD$^+$ ratios close to those of the 'Peredox' plants, some showed substantial increases. In particular, the single knock-down groups 'G' and 'M' showed significant increases in the average NADH/NAD$^+$ ratios with respect to the 'Peredox' plants (Figure 5). The number of plants analysed for c-Peredox-mCherry fluorescence from the double mutant group 'GM' was insufficient to determine if the combination of reduced transcript levels for *NtGAPC* and *NtmMDH* led to significant changes in the NADH/NAD$^+$ ratio.

[COLOUR: PRINT AND ONLINE] Figure 5. Analysis of NAD(H) redox perturbations in the multi-transgene tobacco plants. The NADH/NAD$^+$ ratio, represented as log$_{10}$(tS/mC) was determined based on the fluorescence of the biosensor c-Peredox-mCherry on three-week-old plants. Plants carrying the LS0207 construct, labelled as 'Peredox' were included as controls. Data represent the mean of the expression group ± standard error. Colouring represents groups based on transcript levels, as per Figure 3. Significant changes between groups were identified by one-way ANOVA, followed by post hoc Tukey multiple pairwise comparisons test. P-value = 0.0003.
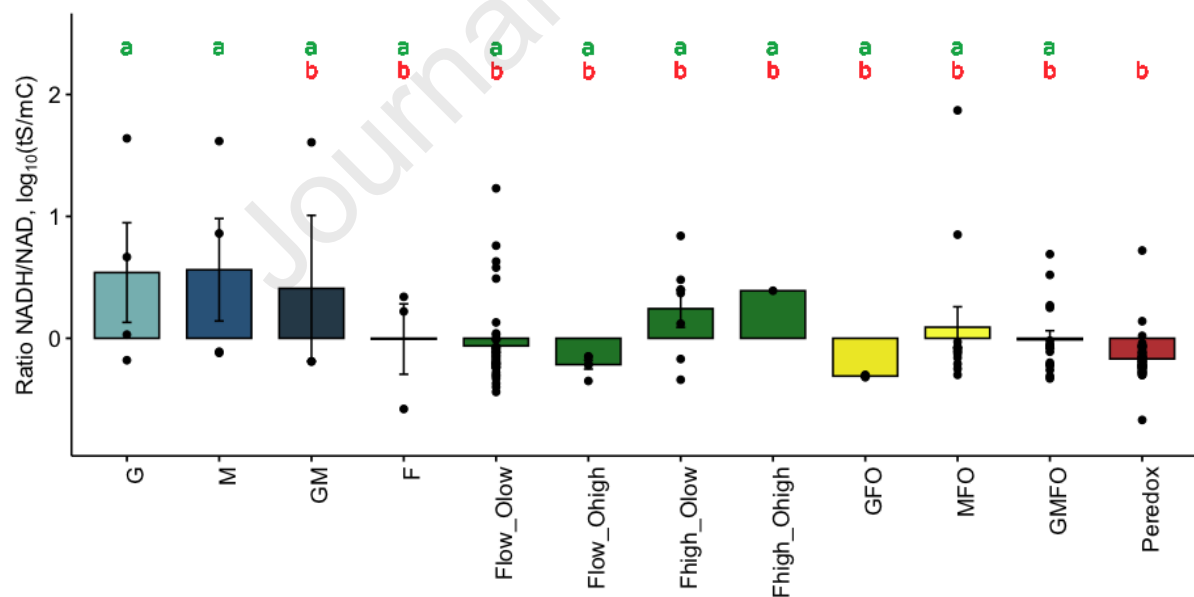
Average transcript levels in the multi-transgene tobacco plants correlate negatively with plant growth and chlorophyll fluorescence-derived parameters

To investigate if variations in transcript levels of the transgenes or silenced genes were linked to variations in the parameters measured, two types of analysis were done. First, PCA was used as a multivariate analysis in an attempt to reduce the dimensions of the dataset. For this analysis, the dataset containing the measured values for a total of 45 parameters in the multi-transgene plants (LS0201), Peredox plants (LS0207), and WT controls was used. Five principal components (PC) explained 84% of the variance (Figure 6.A). Figures 6.B and 6.C represent the category and expression group of, respectively, the top 10 variables (measured parameters) and individuals (transgenic and control plants) contributing to PC1 to PC5. The contribution of the top 10 variables and individuals to PC1 to PC5 can be found in Supplementary Tables 4 and 5, with the top parameters contributing to a certain PC expected to increase together. The first PC (PC1, 31% of variance explained) had large positive associations with several chlorophyll-fluorescence parameters, including F_v/F_m (Figure 6.B, Supplementary Table 4). The second PC (PC2, 28% of variance explained) primarily measured chlorophyll-fluorescence, including performance index on absorption basis, and growth-related parameters, including stem and total biomass, and height. The third PC (PC3, 9% of variance explained) increased with transcript levels of the overexpressed genes *AtFIS1A* and *AtpOMT1* and fluorescence of c-Peredox-mCherry (Ts and mC). PC4 (8% of variance explained) had large positive associations with plant growth parameters (biomass components and total number of leaves) and transcript levels of the overexpressed gene *AtpOMT1.* Finally, PC5 (7% of variance explained) was primarily associated with expression of the silenced genes *NtGAPC* and *NtmMDH* and certain chlorophyll-fluorescence parameters (Figure 6.B, Supplementary Table 4).

When exploring the contributions of each individual to different PCs (Figure 6.C, Supplementary Table 5), it could be seen that the top contributors to PC1 and PC2 were a plant from the 'GM' expression group and plants from the 'M' and 'G' group, followed by several 'Peredox' plants. This suggests a possible link between the knock-down of *NtGAPC* and *NtmMDH* and certain chlorophyll fluorescence and growth parameters. The 'G', 'M' and 'GM' groups showed the highest values for F_v/F_m and total aerial biomass (Figure 4), although these increases were not significant with respect to the controls. It was revealed from PC4 that the top contributing plants had high transcript levels for *AtpOMT* (groups 'Fhigh_Ohigh' and 'GMFO'), implying a correlation between the expression of this transgene and biomass parameters. The presence of 'Peredox' plants across the different PCs suggests high variability within these plants, as seen in Figure 4.

[COLOUR: PRINT AND ONLINE] Figure 6. Principal component analysis of the parameters measured in the multi-transgene tobacco plants. A. Scree plot showing the percentage of variance explained by each principal component (PC). Contributions of variables (**B**) and individuals (**C**) to each PC in the PCA analysis of the multi-transgene transgenic tobacco plants. The categories (variables) and expression groups (individuals) are represented for the top ten contributors are represented.
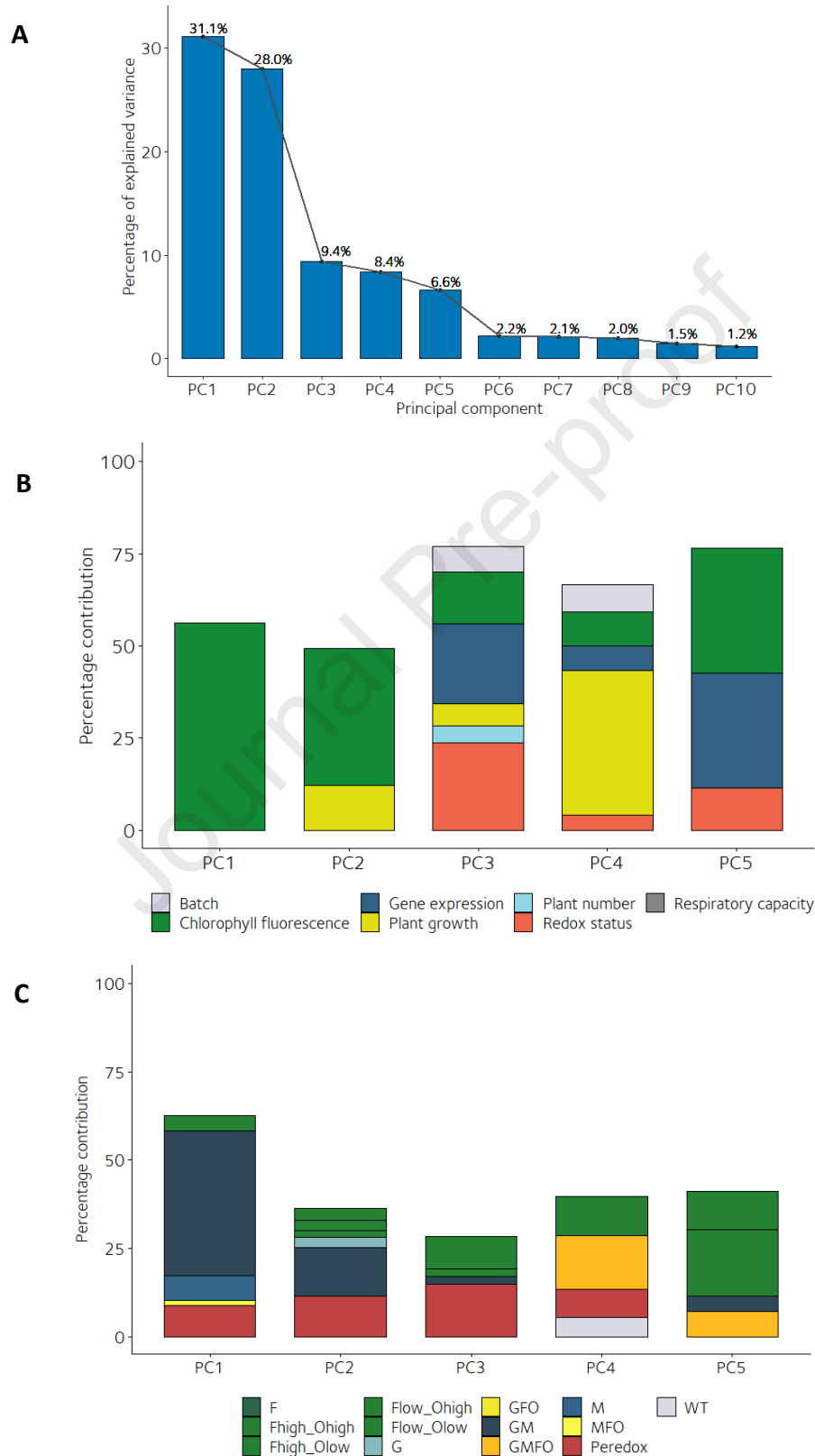
Next, correlations between transgene expression and redox status, respiratory, physiological, and photosynthetic parameters were explored using a Spearman correlation test. Transcript levels for each transgene were converted to log_{10} values and averaged. Supplementary Table 6 summarises the correlation coefficients and significance for each correlation test. Moderate but significant (p-value < 0.05) negative correlations were observed between average transcript levels and the $NADH/NAD^+$ ratio (R = −0.22), plant height (R = −0.37), and stem biomass (R = −0.31). No correlation was found between transcript levels and oxygen consumption rates (R = −0.17) (Supplementary Table 6).

Most chlorophyll fluorescence parameters, extracted from the OJIP transient, showed significant correlations with transcript levels (Supplementary Table 6). A moderate negative correlation was observed between transcript levels and overall photosynthetic capacity, particularly with the maximum quantum yield of PS II photochemistry (R = −0.45), quantum yield of electron transport from quinone to the plastoquinone pool (R = −0.38) and performance index of PS II (R = −0.35). On the other hand, a moderately positive correlation was found with energy dissipation as heat (R = 0.45) and photosynthetic parameters related to specific energy fluxes through the electron transport chain, i.e. apparent antenna size per active PS II (R = 0.43), maximum trapped exciton flux per active PS II (R = 0.38), and the flux of energy dissipated in processes other than trapping per active PS II (R = 0.43).

Correlations between transcript levels and certain photosynthetic parameters and plant growth were also inferred in the PCA analysis, where the top contributing variables to PC1 and PC2 (primarily measuring chlorophyll-fluorescence and plant growth parameters) were plants with reduced levels of *NtGAPC* and *NtmMDH* (Supplementary Table 5). Also, transcript levels of *AtpOMT1* increased together with plant growth parameters in PC4 (Figure 6.B, Supplementary Table 4).

Discussion

The contribution of selected targets to the energetic and redox coupling between organelles

This work explored the effects of altering the exchange of energy and redox equivalents between organelles in leaves using a multi-transgene engineering approach. Our findings suggested a negative association between transcript levels and plant height, stem biomass, photosynthetic capacity, and the cytosolic NADH/NAD^+ ratio.

The *in vivo* monitoring of cytosolic NAD redox changes with c-Peredox-mCherry was recently tested in response to light, sugars, and photosynthetic and respiratory inhibitors in Arabidopsis (Steinbeck *et al.*, 2020). The authors showed that cytosolic NADH/NAD^+ ratios increased in response to light and to the mitochondrial complex III inhibitor antimycin A. The response to light was lost when photosystem II inhibitor 3-(3,4-di- chlorophenyl)-1,1-dimethylurea (DCMU) was applied, which means the reduction of the cytosolic NAD^+ pool in response to light was a consequence of photosynthetic activity (Steinbeck *et al.*, 2020).

In this work, the negative correlation between the dark cytosolic NADH/NAD^+ ratio and average transcript levels in the multi-transgene plants might be explained by increased dark respiratory capacity or by decreased photosynthetic capacity. Dark respiration, measured as leaf disc oxygen consumption, remained unchanged in the transgenic plants and did not correlate with average transcript levels. With no changes to dark respiration, the negative correlation between transcript levels and the reduction status of the cytosolic NAD^+ pool is therefore more likely to be explained by an alteration of photosynthetic activity. Given the difficulty of monitoring sensor fluorescence while illuminating the leaf discs, the redox status of the cytosolic NAD^+ pool was measured in the dark, which could mean that any potential reductions in chlorophyll fluorescence were a consequence of an inactive photosynthetic machinery. However, transcript levels correlated negatively with certain chlorophyll fluorescence parameters too. Therefore, it is possible that these negative correlations reflect detrimental effects to photosynthetic activity caused by the introduced transgenes.

Overexpression and suppression of genes will typically have an asymmetric quantitative contribution when expressed as a $\log_{10}$ ratio relative to the WT transcript abundance. This is because overexpression often results in several hundredfold increases in transcript abundance (as demonstrated in the results here, Figure 3 and Supplementary Table 2) while antisense suppression typically leads to at most a 75% decrease in transcript abundance (Figure 3 and Supplementary Table 2). Therefore, when correlating the average transgene expression with the measured parameters, the overexpressed genes are likely to have a disproportionate influence on any statistical correlation. As a result, the observed correlations may be more strongly influenced by the expression of *AtFIS1A* (and its effect on mitochondrial division) and *AtpOMT1* (as part of the malate valve).

Overexpression of the mitochondrial outer membrane protein FISSION1A did not lead to phenotypic differences in Arabidopsis (Zhang and Hu, 2008), but it is possible that an alteration in mitochondrial number could affect chloroplast activity, similar to the *albolstrians* mutant (Hedtke *et al.*, 1999). Another possibility is that the alteration of the chloroplast malate valve, mediated by overexpression of *AtpOMT1*, negatively affected photosynthetic capacity.

The potential for increased levels of *AtpOMT1* transcripts to explain negative correlations between transcript levels and growth/photosynthetic parameters

The pOMT transporter is thought to be an essential component of the chloroplast malate valve. Arabidopsis mutants in *AtpOMT1* showed increased photoinhibition (increased rate of F_v/F_m decrease after exposure to high light in mutants) due to reducing equivalents accumulating in the stroma, and impaired growth (Kinoshita *et al.*, 2011). Recently, the maize gene coding for pOMT,

ZmOMT1, was overexpressed in rice as part of efforts to introduce C_4 photosynthesis in C_3 crops (Zamani-Nour *et al.*, 2021). The transgenic lines with the highest expression levels showed reduced height and leaf lesions in mature leaves, accompanied by small reductions in CO_2 assimilation rates and increased photorespiration and dark respiration rates (Zamani-Nour *et al.*, 2021). The phenotype was rescued by simultaneously introducing *ZmDiT1* into the *ZmOMT1* transgenic lines, which suggested that defects were caused by an imbalance between the transport of OAA, malate, and 2-oxoglutarate by pOMT1 and glutamate and aspartate by DiT1. Therefore, it is possible that the negative correlations between transcript levels and photosynthetic capacity and growth in the multi-transgene tobacco plants could be related to the overexpression of *AtpOMT1*. This could be inferred from PC4, where the top contributing variables were the transcript levels of *AtpOMT1* and certain plant growth parameters, which suggests an association between the overexpression of *AtpOMT1* and plant growth. While no significant phenotypic changes were observed in the tobacco multi-transgene plants, it is possible that the potential detrimental effects brought about by the overexpression *AtpOMT1* were counteracted by other genetic alterations in the transgenic plants. More specifically, the silencing of GAPC could have balanced out the changes in the chloroplast malate valve by reducing the export of reducing equivalents from the chloroplast to the cytosol.

The importance of the export of energy and reducing equivalents in the dark, as per the changes in the NADH/NAD$^+$ cytosolic ratios in specific groups

An important finding was that multi-transgene plants where *NtGAPC* or *NtmMDH* were suppressed (groups 'G' and 'M'), showed significant increases in the dark NADH/NAD$^+$ ratios with respect to the 'Peredox' group. This is consistent with recent findings where c-Peredox-mCherry was introduced in the Arabidopsis mutants *mmdh1*, *mmdh2*, and *NADP-mdh* (involved in the chloroplast malate valve). These mutants showed an increased NADH/NAD$^+$ ratio in the dark with respect to the Peredox control (Elsässer *et al.*, 2020). The magnitude of the change was markedly higher in the multi-transgene tobacco plants than in the Arabidopsis mutants, but there was less variability in the Arabidopsis data. These results suggest a high importance for the mitochondrial malate valve and the chloroplast TPT in the export of reducing equivalents and energy in the dark. The number of plants that had knock-down levels of both *NtGAPC* and *NtmMDH* (group 'GM') was insufficient to determine if the double knock-down had a similar effect in the NAD(H) redox status as the individual mutants. The fact that this metabolic phenotype is not observed in plants where *AtFIS1A* is overexpressed suggests that increasing the mitochondrial number may compensate for the lack of mMDH activity in groups 'GMFO' and 'MFO'.

Discussion of the results in the context of the current (rather limited) understanding of energy and redox coupling of leaf organelles

This work set out to investigate inter-organellar energy and redox communication by implementing a multi-transgene approach in tobacco that included the redox biosensor c-Peredox-mCherry. The use of this sensor was key to better understand the changes brought about by the introduced genetic manipulations. Future work could take advantage of inhibitors of mitochondrial and chloroplast activity or other fluorescent sensors that would allow monitoring of further parameters, such as iNAP for NADPH (Tao *et al.*, 2017) or ATeam1.03-nD/nA for MgATP^{2-} sensing (De Col *et al.*, 2017).

Our approach was based around an attempt to generate increased mitochondrial respiratory capacity and alterations to the shuttling of energy and reducing equivalents between organelles. Despite the lack of changes in dark respiratory capacity in the transgenic plants with respect to the controls, the analysis of these tobacco plants suggests that the multi-transgene strategy was successful in altering the inter-organellar cross-talk between chloroplasts and mitochondria, as evidenced by alterations in the redox status of the cytosolic NAD pool, and the correlations between transcript levels and the measured parameters. It remains unclear whether overexpression of

AtFIS1A failed to increase mitochondrial respiratory capacity or whether this was compensated for by the other transgenes or intrinsic metabolic changes. Alternative genes that could replace *AtFIS1A* would be the regulators of mitochondrial biogenesis *HAP4* and *SAK1*, whose overexpression has been shown to increase the levels of mETC proteins and OCR in yeast (Knupp, Arvan and Chang, 2019).

While our analyses were limited to variations in transcript levels, the results of this study provide an insight into the mechanisms of organelle communication, suggesting an important role for the export of reducing equivalents in the dark and for pOMT in maintaining the activity of the chloroplast malate valve. This work highlights the need for careful consideration of the cellular energy and redox balance when implementing future metabolic engineering strategies.

References

- Alber, N. A. and Vanlerberghe, G. C. (2019) 'Signaling interactions between mitochondria and chloroplasts in *Nicotiana tabacum* leaf', *Physiologia Plantarum*, 167(2), pp. 188–204. doi: 10.1111/ppl.12879.
- Alber, N. A. and Vanlerberghe, G. C. (2021) 'The flexibility of metabolic interactions between chloroplasts and mitochondria in *Nicotiana tabacum* leaf', *The Plant Journal*, pp. 0–2. doi: 10.1111/tpj.15259.
- Amthor, J. S. (2010) 'From sunlight to phytomass: On the potential efficiency of converting solar radiation to phyto-energy', *New Phytologist*, 188(4), pp. 939–959. doi: 10.1111/j.1469-8137.2010.03505.x.
- Araújo, W. L. *et al.* (2011) 'Antisense inhibition of the iron-sulphur subunit of succinate dehydrogenase enhances photosynthesis and growth in tomato via an organic acid-mediated effect on stomatal aperture', *The Plant Cell*, 23(2), pp. 600–627. doi: 10.1105/tpc.110.081224.
- Baghalian, K., Hajirezaei, M. R. and Schreiber, F. (2014) 'Plant metabolic modeling: Achieving new insight into metabolism and metabolic engineering', *The Plant Cell*, 26(10), pp. 3847–3866. doi: 10.1105/tpc.114.130328.
- Bailleul, B. *et al.* (2015) 'Energetic coupling between plastids and mitochondria drives CO_2 assimilation in diatoms', *Nature*, 524(7565), pp. 366–369. doi: 10.1038/nature14599.
- Barreto, P. *et al.* (2017) 'Mitochondrial uncoupling protein 1 overexpression increases yield in *Nicotiana tabacum* under drought stress by improving source and sink metabolism', *Frontiers in Plant Science*, 8(Nov), pp. 1–20. doi: 10.3389/fpls.2017.01836.
- Bartoli, C. G. *et al.* (2005) 'Up-regulation of the mitochondrial alternative oxidase pathway enhances photosynthetic electron transport under drought conditions', *Journal of Experimental Botany*, 56(415), pp. 1269–1276. doi: 10.1093/jxb/eri111.
- Beer, C. *et al.* (2010) 'Terrestrial gross carbon dioxide uptake: Global distribution and covariation with climate', *Science*, 329(5993), pp. 834–838. doi: 10.1126/science.1184984.
- Carrari, F. *et al.* (2003) 'Reduced expression of aconitase results in an enhanced rate of photosynthesis and marked shifts in carbon partitioning in illuminated leaves of wild species tomato', *Plant Physiology*, 133(3), pp. 1322–1335. doi: 10.1104/pp.103.026716.
- De Col, V. *et al.* (2017) 'ATP sensing in living plant cells reveals tissue gradients and stress dynamics of energy physiology', *eLife*, 6, e26770. doi: 10.7554/eLife.26770.
- Dahal, K. *et al.* (2017) 'Coordinated regulation of photosynthetic and respiratory components is necessary to maintain chloroplast energy balance in varied growth conditions', *Journal of Experimental Botany*, 68(3), pp. 657–671. doi: 10.1093/jxb/erw469.
- Dahal, K. and Vanlerberghe, G. C. (2018) 'Improved chloroplast energy balance during water deficit enhances plant growth: More crop per drop', *Journal of Experimental Botany*, 69(5), pp. 1183–1197. doi: 10.1093/jxb/erx474.
- Dutilleul, C. *et al.* (2003) 'Functional mitochondrial complex I is required by tobacco leaves for optimal photosynthetic performance in photorespiratory conditions and during transients', *Plant Physiology*, 131(1), pp. 264–275. doi: 10.1104/pp.011155.
- Elsässer, M. *et al.* (2020) 'Photosynthetic activity triggers pH and NAD redox signatures across different plant cell compartments', *bioRxiv*, p. 2020.10.31.363051. doi:

10.1101/2020.10.31.363051.

- Engler, C. *et al.* (2009) 'Golden gate shuffling: A one-pot DNA shuffling method based on type ils restriction enzymes', *PLoS ONE*, 4(5), e5553. doi: 10.1371/journal.pone.0005553.
- Engler, C. *et al.* (2014) 'A golden gate modular cloning toolbox for plants', *ACS Synthetic Biology*, 3(11), pp. 839–843. doi: 10.1021/sb4001504.
- Engler, C., Kandzia, R. and Marillonnet, S. (2008) 'A one pot, one step, precision cloning method with high throughput capability', *PLoS ONE*, 3(11), e3647. doi: 10.1371/journal.pone.0003647.
- Fernandez-Pozo, N. *et al.* (2015) 'The Sol Genomics Network (SGN)-from genotype to phenotype to breeding', *Nucleic Acids Research*, 43(D1), pp. D1036–D1041. doi: 10.1093/nar/gku1195.
- Fuentes, D. *et al.* (2011) 'A deficiency in the flavoprotein of Arabidopsis mitochondrial complex II results in elevated photosynthesis and better growth in nitrogen-limiting conditions.', *Plant Physiology*, 157(3), pp. 1114–27. doi: 10.1104/pp.111.183939.
- Gardeström, P. and Igamberdiev, A. U. (2016) 'The origin of cytosolic ATP in photosynthetic cells', *Physiologia Plantarum*, 157(3), pp. 367–379. doi: 10.1111/ppl.12455.
- Hatch, M. D. *et al.* (1984) 'A specific translocator for oxaloacetate transport in chloroplasts', *FEBS Letters*, 178(1), pp. 15–19. doi: 10.1016/0014-5793(84)81230-2.
- Häusler, R. E. *et al.* (2000) 'Control of carbon partitioning and photosynthesis by the triose phosphate/phosphate translocator in transgenic tobacco plants (*Nicotiana tabacum* L.). I. Comparative physiological analysis of tobacco plants with antisense repression and overexpression of the triose phosphate/phosphate translocator', *Planta*, 210(3), pp. 371–382. doi: 10.1007/PL00008145.
- Hedtke, B. *et al.* (1999) 'Inter-organellar crosstalk in higher plants: Impaired chloroplast development affects mitochondrial gene and transcript levels', *The Plant Journal*, 19(6), pp. 635–643. doi: 10.1046/j.1365-313X.1999.00554.x.
- Horsch, R. B. *et al.* (1985) 'A simple and general method for transferring genes into plants', *Science*, 227(4691), pp. 1229–1230. doi: 10.1126/science.227.4691.1229.
- Hung, Y. P. *et al.* (2011) 'Imaging cytosolic NADH-NAD+ redox state with a genetically encoded fluorescent biosensor', *Cell Metabolism*, 14(4), pp. 545–554. doi: 10.1016/j.cmet.2011.08.012.
- Igamberdiev, A. U. *et al.* (1998) 'The role of mitochondrial electron transport during photosynthetic induction. A study with barley (*Hordeum vulgare*) protoplasts incubated with rotenone and oligomycin', *Physiologia Plantarum*, 104(3), pp. 431–439. doi: 10.1034/j.1399-3054.1998.1040319.x.
- Kinoshita, H. *et al.* (2011) 'The chloroplastic 2-oxoglutarate/malate transporter has dual function as the malate valve and in carbon/nitrogen metabolism', *The Plant Journal*, 65(1), pp. 15–26. doi: 10.1111/j.1365-313X.2010.04397.x.
- Knupp, J., Arvan, P. and Chang, A. (2019) 'Increased mitochondrial respiration promotes survival from endoplasmic reticulum stress', *Cell Death and Differentiation*, 26(3), pp. 487-501. doi: 10.1038/s41418-018-0133-4.
- Kromer, S. (1995) 'Respiration during photosynthesis', *Annual Review of Plant Physiology and Plant Molecular Biology*, 46, pp. 45–70. doi: 10.1146/annurev.pp.46.060195.000401.
- Laitz, A. V. N. *et al.* (2015) 'Transcriptome response signatures associated with the

overexpression of a mitochondrial uncoupling protein (AtUCP1) in tobacco', *PLoS ONE*, 10(6), pp. 1–19. doi: 10.1371/journal.pone.0130744.

- Lim, S. L. *et al.* (2020) '*In planta* study of photosynthesis and photorespiration using NADPH and NADH/NAD+ fluorescent protein sensors', *Nature Communications*, 11(1). doi: 10.1038/s41467-020-17056-0.

- Lindén, P. *et al.* (2016) 'Reduced mitochondrial malate dehydrogenase activity has a strong effect on photorespiratory metabolism as revealed by ^{13}C labelling', *Journal of Experimental Botany*, 67(10), pp. 3123–3135. doi: 10.1093/jxb/erw030.

- McDonald, A. E. and Vanlerberghe, G. C. (2007) 'The organization and control of plant mitochondrial metabolism', *Annual Plant Reviews*, 22, pp. 290–324. doi: 10.1002/9780470988640.ch11.

- Müller-Schüssele, S. J., Schwarzländer, M. and Meyer, A. J. (2021) 'Live monitoring of plant redox and energy physiology with genetically encoded biosensors', *Plant Physiology*, 186(1), pp. 93–109. doi: 10.1093/plphys/kiab019.

- Noctor, G., De Paepe, R. and Foyer, C. H. (2007) 'Mitochondrial redox biology and homeostasis in plants', *Trends in Plant Science*, 12(3), pp. 125–134. doi: 10.1016/j.tplants.2007.01.005.

- Nunes-Nesi, A. *et al.* (2005) 'Enhanced photosynthetic performance and growth as a consequence of decreasing mitochondrial malate dehydrogenase activity in transgenic tomato plants.', *Plant Physiology*, 137(2), pp. 611–22. doi: 10.1104/pp.104.055566.

- Nunes-Nesi, A. *et al.* (2007) 'Deficiency of mitochondrial fumarase activity in tomato plants impairs photosynthesis via an effect on stomatal function', *The Plant Journal*, 50(6), pp. 1093–1106. doi: 10.1111/j.1365-313X.2007.03115.x.

- Nunes-Nesi, A. *et al.* (2008) 'The enigmatic contribution of mitochondrial function in photosynthesis', *Journal of Experimental Botany*, 59(7), pp. 1675–1684. doi: 10.1093/jxb/ern002.

- Nunes-Nesi, A., Sweetlove, L. J. and Fernie, A. R. (2007) 'Operation and function of the tricarboxylic acid cycle in the illuminated leaf', *Physiologia Plantarum*, 129(1), pp. 45–56. doi: 10.1111/j.1399-3054.2006.00778.x.

- O'Leary, B. M. *et al.* (2017) 'Variation in leaf respiration rates at night correlates with carbohydrate and amino acid supply', *Plant Physiology*, 174(4), pp. 2261–2273. doi: 10.1104/pp.17.00610.

- Padmasree, K., Padmavathi, L. and Raghavendra, A. S. (2002) 'Essentiality of mitochondrial oxidative metabolism for photosynthesis: Optimization of carbon assimilation and protection against photoinhibition', *Critical Reviews in Biochemistry and Molecular Biology,* 37(2):71-119. doi: 10.1080/10409230290771465.

- Padmasree, K. and Raghavendra, A. S. (2001) 'Consequence of restricted mitochondrial oxidative metabolism on photosynthetic carbon assimilation in mesophyll protoplasts: Decrease in light activation of four chloroplastic enzymes', *Physiologia Plantarum*, 112(4), pp. 582–588. doi: 10.1034/j.1399-3054.2001.1120417.x.

- Peremarti, A. *et al.* (2010) 'Promoter diversity in multigene transformation'. *Plant Molecular Biology* 73(4-5):363–378. doi: 10.1007/s11103-010-9628-1.

- Pfaffl, M. W. (2001) 'A new mathematical model for relative quantification in real-time RT-PCR', *Nucleic Acids Research*, 29(9), pp. 2003–2007. doi: 10.1093/nar/29.9.e45.

- R Development Core Team (2013) 'R: A language and environment for statistical computing.', *R Foundation for Statistical Computing, Vienna, Austria.*

- Rius, S. P. *et al.* (2008) 'Characterization of Arabidopsis lines deficient in GAPC-1, a cytosolic NAD-dependent glyceraldehyde-3-phosphate dehydrogenase', *Plant Physiology*, 148(3), pp. 1655–1667. doi: 10.1104/pp.108.128769.
- RStudio Team (2020) 'RStudio: Integrated Development Environment for R', *RStudio, PBC*.
- Schmidt, G. W. and Delaney, S. K. (2010) 'Stable internal reference genes for normalization of real-time RT-PCR in tobacco (*Nicotiana tabacum*) during development and abiotic stress', *Molecular Genetics and Genomics*, 283(3), pp. 233–241. doi: 10.1007/s00438-010-0511-1.
- Schneider, A. *et al.* (2002) 'An *Arabidopsis thaliana* knock-out mutant of the chloroplast triose phosphate/phosphate translocator is severely compromised only when starch synthesis, but not starch mobilisation is abolished', *The Plant Journal*, 32(5), pp. 685–699. doi: 10.1046/j.1365-313X.2002.01460.x.
- Schwarzländer, M. *et al.* (2016) 'Dissecting redox biology using fluorescent protein sensors', *Antioxidants and Redox Signaling*, 24(13), pp. 680–712. doi: 10.1089/ars.2015.6266.
- Selinski, J. and Scheibe, R. (2019) 'Malate valves: old shuttles with new perspectives', *Plant Biology*, 21, pp. 21–30. doi: 10.1111/plb.12869.
- Sew, Y. S. *et al.* (2013) 'Multiplex micro-respiratory measurements of Arabidopsis tissues', *New Phytologist*, 200(3), pp. 922–932. doi: 10.1111/nph.12394.
- Sew, Y. S., Harvey Millar, A. and Stroeher, E. (2015) 'Micro-respiratory measurements in plants', in *Plant Mitochondria: Methods and Protocols*. Springer New York, pp. 187–196. doi: 10.1007/978-1-4939-2639-8_13.
- Shameer, S. *et al.* (2018) 'Computational analysis of the productivity potential of CAM', *Nature Plants*, 4(3), pp. 165–171. doi: 10.1038/s41477-018-0112-2.
- Shameer, S., Ratcliffe, R. G. and Sweetlove, L. J. (2019) 'Leaf energy balance requires mitochondrial respiration and export of chloroplast NADPH in the light', *Plant Physiology*, 180(4), pp. 1947–1961. doi: 10.1104/pp.19.00624.
- Smith, E. N. *et al.* (2021) 'Shining a light on NAD- and NADP-based metabolism in plants', *Trends in Plant Science*, [in press]. doi: 10.1016/j.tplants.2021.06.010.
- Steinbeck, J. *et al.* (2020) 'In vivo NADH/NAD+ biosensing reveals the dynamics of cytosolic redox metabolism in plants', *The Plant Cell*, 32, pp. 3324–3345. doi: 10.1105/tpc.20.00241.
- Strasser, R. J., Srivastava, A. and Tsimilli-Michael, M. (2000) 'The fluorescence transient as a tool to characterize and screen photosynthetic samples', in M., Y., Pathre, U., and Mohanty, P. (eds) *Probing Photosynthesis: Mechanism, Regulation and Adaptation*. Taylor & Francis, pp. 445–483. doi: 10.1016/S0269-7491(03)00094-0.
- Sweetlove, L. J. *et al.* (2006) 'Mitochondrial uncoupling protein is required for efficient photosynthesis.', *Proceedings of the National Academy of Sciences of the United States of America*, 103(51), pp. 19587–92. doi: 10.1073/pnas.0607751103.
- Sweetlove, L. J. *et al.* (2007) 'The mitochondrion: An integration point of cellular metabolism and signalling', *Critical Reviews in Plant Sciences*, 26(1), pp. 17–43. doi: 10.1080/07352680601147919.
- Sweetlove, L. J. *et al.* (2013) 'Modelling metabolic CO_2 evolution - A fresh perspective on respiration', *Plant, Cell and Environment*, 36(9), pp. 1631–1640. doi: 10.1111/pce.12105.
- Taniguchi, M. *et al.* (2002) 'Identifying and characterizing plastidic 2-

oxoglutarate/malate and dicarboxylate transporters in *Arabidopsis thaliana*', *Plant and Cell Physiology*, 43(7), pp. 706–717. doi: 10.1093/pcp/pcf109.

- Taniguchi, M. and Miyake, H. (2012) 'Redox-shuttling between chloroplast and cytosol: Integration of intra-chloroplast and extra-chloroplast metabolism', *Current Opinion in Plant Biology*, 15(3), pp. 252–260. doi: 10.1016/j.pbi.2012.01.014.

- Tao, R. *et al.* (2017) 'Genetically encoded fluorescent sensors reveal dynamic regulation of NADPH metabolism', *Nature Methods*, 14(7), pp. 720–728. doi: 10.1038/nmeth.4306.

- Tomaz, T. *et al.* (2010) 'Mitochondrial malate dehydrogenase lowers leaf respiration and alters photorespiration and plant growth in Arabidopsis', *Plant Physiology*, 154(3), pp. 1143–1157. doi: 10.1104/pp.110.161612.

- Vanlerberghe, G. C. *et al.* (2020) 'Photosynthesis, respiration and growth: A carbon and energy balancing act for alternative oxidase', *Mitochondrion*, 52, pp. 197–211. doi: 10.1016/j.mito.2020.04.001.

- Voon, C. P. *et al.* (2018) 'ATP compartmentation in plastids and cytosol of *Arabidopsis thaliana* revealed by fluorescent protein sensing', *Proceedings of the National Academy of Sciences of the United States of America*, 115(45), pp. E10778–E10787. doi: 10.1073/pnas.1711497115.

- Wagner, S. *et al.* (2019) 'Multiparametric real-time sensing of cytosolic physiology links hypoxia responses to mitochondrial electron transport', *New Phytologist*, 224(4), pp. 1668–1684. doi: 10.1111/nph.16093.

- Weber, E. *et al.* (2011) 'A modular cloning system for standardized assembly of multigene constructs', *PLoS ONE*, 6(2), e16765. doi: 10.1371/journal.pone.0016765.

- Xu, Y. *et al.* (2021) 'The metabolic origins of non-photorespiratory CO_2 release during photosynthesis: A metabolic flux analysis', *Plant Physiology,* 186(1), pp. 297-314. doi: 10.1093/plphys/kiab076.

- Zamani-Nour, S. *et al.* (2021) 'Overexpression of the chloroplastic 2-oxoglutarate/malate transporter disturbs carbon and nitrogen homeostasis in rice', *Journal of Experimental Botany*, 72(1), pp. 137–152. doi: 10.1093/jxb/eraa343.

- Zhang, X. C. and Hu, J. P. (2008) 'FISSION1A and FISSION1B proteins mediate the fission of peroxisomes and mitochondria in Arabidopsis', *Molecular Plant*, 1(6), pp. 1036–1047. doi: 10.1093/mp/ssn056.

- Zhang, X. C. and Hu, J. P. (2009) 'Two small protein families, DYNAMIN-RELATED PROTEIN3 and FISSION1, are required for peroxisome fission in Arabidopsis', *The Plant Journal*, 57(1), pp. 146–159. doi: 10.1111/j.1365-313X.2008.03677.x.

- A multi-transgene construct targeted tobacco leaf redox and energy metabolism.
- Average transcript levels correlated negatively with plant growth and photosynthesis.
- Overexpression of chloroplast malate valve transporter could explain correlations.
- Redox biosensor c-Peredox-mCherry was used to report cytosolic NADH/NAD$^+$ ratios.
- Defects in mitochondrial and chloroplasts shuttles increase dark NADH/NAD+ ratios.

We conceived a multi-transgene metabolic engineering strategy to investigate inter-organellar energy and redox coupling in tobacco. Our analyses point towards the overexpression of the chloroplast malate valve transporter pOMT as a negative contributor to several chlorophyll fluorescence and plant growth parameters. In addition, our findings suggest an important role for mitochondrial and malate shuttles for redox balancing in the dark as knocking down the cytosolic NAD-dependent glyceraldehyde 3-phosphate dehydrogenase (GAPC) and the mitochondrial NAD-malate dehydrogenase (mMDH) led to a higher cytosolic NADH/NAD$^+$ ratio. This work highlights the need for careful consideration of the cellular energy and redox balance when implementing future metabolic engineering strategies.

Declaration of interests

☒ The authors declare that they have no known competing financial interests or personal relationships that could have appeared to influence the work reported in this paper.

☐The authors declare the following financial interests/personal relationships which may be considered as potential competing interests: